Metrol. Meas. Syst., Vol. 24 (2017), No. 1, pp. 101–112.

METROLOGY AND MEASUREMENT SYSTEMS

Index 330930, ISSN 0860-8229

www.metrology.pg.gda.pl

KIDNEY SEGMENTATION IN CT DATA USING HYBRID LEVEL-SET METHOD WITH ELLIPSOIDAL SHAPE CONSTRAINTS

Andrzej Skalski[1)], Katarzyna Heryan[1)], Jacek Jakubowski[2)], Tomasz Drewniak[3)]

1) AGH University of Science and Technology, Department of Measurement and Electronics, Al. Mickiewicza 30, Cracow, Poland (✉ skalski@agh.edu.pl, +48 12 617 2828, heryan@agh.edu.pl)

2) Rydygier Memorial Hospital, Department of Urology, Os. Zlotej Jesieni 1, 31-826 Cracow, Poland (jacekjakubowski83@gmail.com)

3) Specialized Municipal Hospital G. Narutowicz, Department of Urology, Prądnicka 35-37, 31-202 Cracow, Poland (tomdrew@vp.pl)

Abstract

With development of medical diagnostic and imaging techniques the sparing surgeries are facilitated. Renal cancer is one of examples. In order to minimize the amount of healthy kidney removed during the treatment procedure, it is essential to design a system that provides three-dimensional visualization prior to the surgery. The information about location of crucial structures (*e.g.* kidney, renal ureter and arteries) and their mutual spatial arrangement should be delivered to the operator. The introduction of such a system meets both the requirements and expectations of oncological surgeons. In this paper, we present one of the most important steps towards building such a system: a new approach to kidney segmentation from Computed Tomography data. The segmentation is based on the Active Contour Method using the *Level Set* (LS) framework. During the segmentation process the energy functional describing an image is the subject to minimize. The functional proposed in this paper consists of four terms. In contrast to the original approach containing solely the region and boundary terms, the ellipsoidal shape constraint was also introduced. This additional limitation imposed on evolution of the function prevents from leakage to undesired regions. The proposed methodology was tested on 10 Computed Tomography scans from patients diagnosed with renal cancer. The database contained the results of studies performed in several medical centers and on different devices. The average effectiveness of the proposed solution regarding the Dice Coefficient and average Hausdorff distance was equal to 0.862 and 2.37 mm, respectively. Both the qualitative and quantitative evaluations confirm effectiveness of the proposed solution.

Keywords: Level Set method, kidney, CT data, image segmentation, ellipsoid.

1. Introduction

Recently, the increase of kidney cancer incidences has been observed. Due to the fact that this type of cancer is frequently diagnosed at an early stage of its development, it is possible to provide the sparing treatment [1]. Its idea is to extract only the tumor lesion with a necessary margin and to remain intact as much of the healthy kidney as possible. This type of treatment requires a precise preoperative planning. For a physician who undertakes the surgery, the information about location of critical structures (kidney, vascular tree, renal pelvis and ureter), their mutual spatial orientation and possible conflicts in the operating field is essential. Therefore, the preoperative imaging, which is in most cases *Computed Tomography* (CT) with a contrast agent, is performed to visualize the structures of interest. Unfortunately, the information presented in this way often appears to be insufficient. It is associated with the kidney spatial arrangement and its geometry, as well as a poor spatial image resolution.

Delivery of a patient-specific three-dimensional model of kidney and other critical structures is indicated as the next step in development of urological oncology [2, 3]. So far only the visualization based solely on the CT data has been used and no reliable automatic tool has been yet proposed. The process of manual preparation of such visualizations is time-consuming

Article history: received on Jun. 07, 2016; accepted on Aug. 28, 2016; available online on Mar. 10, 2017; DOI: 10.1515/mms-2017-0006.

and often inaccurate due to the shift between different data series and insufficient information derived from CT data for such a reconstruction. The optimal approach to facilitate this process seems to be the algorithmic one. In order to make kidney sparing surgery easier, it is important to identify tools for automatic preparation of such a model for each patient. The kidney segmentation, the scope of this paper, is a step on this way. Among the difficulties encountered during the CT data segmentation, there is a slight difference in HU values assigned to the voxels representing the kidney and surrounding tissue. Although several methods for the 3D kidney segmentation have been proposed, they seem to be insufficient for the presented purpose. In general, algorithms of 3D kidney segmentation from the CT data can be divided into 3 main groups:

1. Thresholding, Region Growing and feature extraction methods.
   Lin *et al.* [4] proposed a multistage system. In the first step, location of the spine is used to extract the region candidate. Then, identification the seed point is followed by adaptive region growing. Nedevschi and Mile [5] used a set of texture features derived by Gabor filters and the EM-based image segmentation. Nevertheless, the presented results are coming from 2D slices. These methods are vulnerable to spatial data distribution and dispersion of values; especially present in the case of contrast-enhanced CT data. The data used in our research were of two types: with and without injection of a contrast agent prior to examination.
2. *Atlas and Active Shape/Appearance model* (ASM/AAM) segmentation.
   In [6], the authors proposed a multi-atlas segmentation. The atlas was created using the classical 2D snake segmentation followed by correction made by the radiologist. Xu *et al.* [7] also used the multi-atlas approach. In comparison with the classical multi-atlas strategy, the segmentation was further improved by SIMPLE algorithm with context learning. Chao *et al*. [8] proposed a method for segmentation of kidney compartments. After localization based on Generalized Hough Transform the 3D AAM segmentation is performed. Spiegel *et al.* [9] exploited ASM framework to the kidney segmentation. A crucial correspondence problem in the ASM training phase was solved using the image registration. However, the presented methods require a huge CT database.
3. Active Contours and Level Set segmentation.
   Zolllner *et al.* [10] proposed a 2D Active Contours approach with k-means clustering to provide the initial curve. In [11] the authors introduced the 3D generalization known as Deformable Models. The model is defined by NURBS surfaces constrained by prior statistical information concerning the curvature distribution on the surface. However, this method has a limited robustness to kidney pathologies, which is the case in kidney cancer CT data.
   Khalifa *et al*. used a Level Set method with prior shapes. This methodology was extended by Markov-Gibbs Random Field to model the kidney and surrounding tissues [12]. Huang *et al.* [13] proposed a modification of the Chan-Vese model [14] by using a shape model with kidney variation. Similarly to the methods presented in Section 2, this kind of solution also requires a big database with doctors' manual outlines.

The method proposed in this paper is most congruent with the algorithm presented in [15] for the cardiac MR image segmentation.

2. Methodology

In this section, the background of proposed methodology is given. Subsection 2.1 presents a general framework of kidney segmentation based on the Hybrid Level Set method adopted from [16]. The *Hybrid Level Set* (HLS) extended with the shape constraints is described in Subsections 2.2 and 2.3. Since kidneys have an ellipsoidal shape, this feature was added as

an additional restriction to the evolution equation (Subsection 2.4). In Subsection 2.5, a method of parameter selection is proposed. Finally, in Subsection 2.6 the energy functional minimization process is presented.

2.1. Hybrid Level Set

It was already mentioned in the introduction that our goal is to develop an effective kidney segmentation method from the CT data. The proposed methodology, similarly to that proposed in [15], is based on four major assumptions. First of all, the algorithm should take into account the distribution of values within the object (the region term). The information about the values assigned to the object should be also extended with the boundary information. Moreover, the additional prior knowledge should be introduced, *e.g.* the geometrical model of segmented structure. Finally, smoothness of the resulting kidney contour should be ensured. All of the foregoing assumptions may be included in the *Active Contours* framework.

The idea of image segmentation using *Active Contours* (AC) was introduced in 1988 [17]. Since that time, the researchers have proposed a wide range of AC model modifications. Nonetheless, the AC models are usually based on minimization of the energy functional. The functional is such defined that its smallest value is near or on the target object boundary. In order to solve the minimization problem, a *partial differential equation* (PDE) corresponding to the functional is formulated. From a numerical point of view, the methods for solving this kind of PDE can be divided into three main categories [16]:

- Particle models wherein AC is built of a set of points [17].
- Analytic models in a parametrical form (*e.g.* B-spline [18]).
- *Level Set* (LS) models wherein AC is a zero-level set of functions with an implicit representation defined in a space being by one dimension greater than that of the image [19].

The proposed solution is based on the Level Set model with the boundary information associated with the region information [16].

The preliminary assumptions concerning the proposed solution can be presented in the form of an energy functional $E(C)$ [15]:

$$E(C) = \lambda_1 E_1(C) + \lambda_2 E_2(C) + \lambda_3 E_3(C) + reg\,, \tag{1}$$

where: $E_1(C)$ is the region term; $E_2(C)$ provides information about the boundaries; $E_3(C)$ is the geometrical model of an object and *reg* ensures smoothness of the contour/surface C. The parameter λ_i is the weight of the i-th component impacting the entire functional.

In the LS framework the surface C in the 3-dimensional case is represented as a zero-level set of the function $\Phi(\mathbf{x})$ ($\mathbf{x} = [x_1, x_2, x_3]$) [14, 19]:

$$\begin{cases} C = \{\mathbf{x} \in \Omega : \Phi(\mathbf{x}) = 0\} \\ \Omega_{\text{in}} = \{\mathbf{x} \in \Omega : \Phi(\mathbf{x}) > 0\} \\ \Omega_{\text{out}} = \{\mathbf{x} \in \Omega : \Phi(\mathbf{x}) < 0\} \end{cases}. \tag{2}$$

Using the notation (2), the functional (1) is represented as:

$$E(C) = \lambda_1 E_1(\Phi) + \lambda_2 E_2(\Phi) + \lambda_3 E_3(\Phi) + reg\,. \tag{3}$$

2.2. Region-based term

Contrary to the original approach proposed in [14], here the $E_1(C)$ term is based on the functional component of HLS [16]:

$$E_1(\Phi) = -\int_{\Omega} \big(\mathbf{I}(\mathbf{x}) - \mu\big) H(\Phi) d\Omega\,, \tag{4}$$

where: **I** represents the image data used for segmentation; $H(\Phi)$ is the Heaviside function ($H(\Phi) = 0$ for $\Phi<0$ and $H(\Phi) = 1$ for $\Phi \geq 0$), μ is a parameter indicating the lower threshold value associated with the object, assuming that the object values are relatively higher than those of the background (the method of determining this parameter is described in Subsection 2.5). In consequence of this way of determining (4), the voxels with values greater than μ are preferred [16]. In comparison with the original solution proposed in [14], the number of parameters that require determination is reduced from 2 to 1. Also, this approach eliminates the problem of background/object representation. Moreover, in the kidney surroundings there are voxels with very low values (*e.g.* air in a small intestine or colon), similar values (surrounding soft tissues), *e.g.* the liver, and those with very large ones (*e.g.* bones). Due to such a determination of the boundary term (4), the problem associated with dispersion of the background voxel values is eliminated, which is crucial in this case. In our research, μ parameter was determined prior to segmentation and remained constant during the evolution process.

2.3. Edge-based term

Only if the surrounding structures have similar values and there is a clear boundary between them, the introduction of the image edge information makes the solution more effective. The functional component representing the edge-based term is defined as follows [16]:

$$E_2(\Phi) = \int_{\Omega} \mathbf{g}(\mathbf{x}) \big|\nabla H(\Phi)\big| d\Omega\,, \tag{5}$$

where **g** is the boundary function defined as:

$$\mathbf{g}(\mathbf{x}) = \frac{1}{1 - c\big|\nabla \mathbf{I}(\mathbf{x})\big|^2}\,, \tag{6}$$

where c is a slope control parameter.

2.4. Prior kidney shape term

The major obstacle is that the kidney voxel values are similar to these of the surrounding structures. Moreover, for contrast-enhanced data, sometimes the contrast agent is not propagating as desired, leading to significant dispersion of values within the kidney itself. A similar phenomenon may occur when the image acquisition time is set improperly in relation to the contrast injection.

The proposed solution is based on the 3D generalization of the 2D case presented in [15]. It is modified by adding a functional component representing the object shape. The shape constraint can be provided in several ways. One approach is to use an average shape of the segmented structure with its acceptable variability. Its significant limitation concerns the requirement for a greatly expanded image database describing the kidney and both its geometric and volumetric variations. Another solution that we propose, is to use the feature of kidney similarity to the ellipsoidal shape. An ellipsoid in the three-dimensional space can be described using the quadratic form:

$$a_{11}x_1^2 + a_{22}x_2^2 + a_{33}x_3^2 + a_{12}x_1x_2 + a_{23}x_2x_3 + a_{13}x_1x_3 + a_{14}x_1 + a_{24}x_2 + a_{34}x_3 + a_{44} = 0\,. \tag{7}$$

Or, in a more compact form:

$$\boldsymbol{a}^T \boldsymbol{z} = 0\,, \tag{8}$$

where: $\mathbf{a}^T = [a_{11}, a_{22}, a_{33}, a_{12}, a_{23}, a_{13}, a_{14}, a_{24}, a_{34}, a_{44}]$, $\mathbf{z}^T = [x_1^2, x_2^2, x_3^2, x_1x_2, x_2x_3, x_1x_3, x_1, x_2, x_3, 1]$.

In this case, the crucial issue is to ensure that (8) will be indeed an ellipsoid. The conditions for it are as follows [20, 21]:

$$4\left(a_{11}a_{22}+a_{22}a_{33}+a_{11}a_{33}-\frac{1}{4}a_{12}^2-\frac{1}{4}a_{23}^2-\frac{1}{4}a_{13}^2\right)-\left(a_{11}+a_{22}+a_{33}\right)^2>0,\ 4M-L>0. \quad (9)$$

If $4M-L>0$, the vector of searching parameters **a** represents an ellipsoid. Based on this, it is possible to formulate an optimization problem: $\min_{\mathbf{a}} \mathbf{a}^T\mathbf{R}\mathbf{a}$ and $\mathbf{a}^T\mathbf{Q}\mathbf{a}=1$, where the matrix **R** represents points belonging to the zero-level set of Φ and **Q** is a constraint matrix presented in [20]:

$$\mathbf{Q}=\mathrm{diag}\left(-\frac{1}{2}k\left(\begin{bmatrix}1&1&1\\1&1&1\\1&1&1\end{bmatrix}+\begin{bmatrix}1&0&0\\0&1&0\\0&0&1\end{bmatrix}\right),-\frac{1}{4}k\begin{bmatrix}1&0&0\\0&1&0\\0&0&1\end{bmatrix},\begin{bmatrix}0&0&0&0\\0&0&0&0\\0&0&0&0\\0&0&0&0\end{bmatrix}\right), \quad (10)$$

where $k\geq 4$. More details and a fitting procedure can be found in [20].

After estimation of the vector **a**, another level-set function **D** representing the distance to the ellipsoid surface can be specified. **D** can be calculated in two ways:

$$\mathbf{D}_I=d;\ \mathbf{D}_{II}=\begin{cases}d & \text{outside ellipsoid}\\ 0 & \text{inside ellipsoid}\end{cases}, \quad (11)$$

where d is a distance to the ellipsoid equal to $\mathbf{a}^T\mathbf{z}$. $\mathbf{D}_I$ prefers the external surface as the final result, whereas $\mathbf{D}_{II}$ allows for topological changes inside the ellipsoid. By using $\mathbf{D}_{II}$ the inner structure of kidney can be differentiated. The results of the segmentation process depending on choosing either $\mathbf{D}_I$ or $\mathbf{D}_{II}$ are presented in Fig. 1.

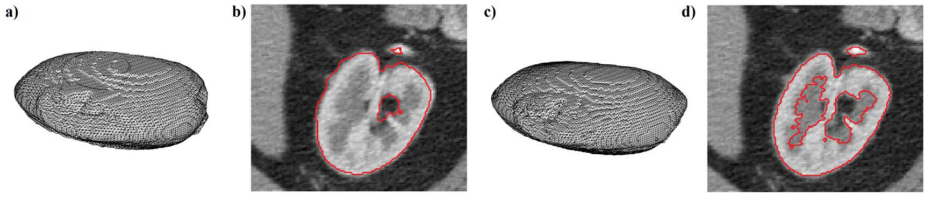

Fig. 1. An example of the results with $\mathbf{D}_I$, (a) and (b), $\mathbf{D}_{II}$ (c), and (d) the formulation used in (12); (a), (c) the final kidney surface; (b), (d) the result (red contour) on the slice through (a) and (c).

Finally, $E_3(C)$ can be determined:

$$E_3(\Phi)=\int_{\Omega}\mathbf{D}^2(\mathbf{x})\left|\nabla H(\Phi)\right|d\Omega. \quad (12)$$

2.5. Estimation of μ

The value of μ parameter can be obtained by different methods. The simplest possible way is its indication based on thresholding or manual histogram analysis. Automatic results can be achieved by interpretation of normalized histogram function approximation parameters. For this purpose, in this study, the approximation of normalized histogram is performed by the *Gaussian Mixture Model* (GMM) using the iterative Expectation-Maximization algorithm [22].

GMM consists of k Gaussian functions. Each function is parameterized by $\overline{\mathbf{w}}_i$ that represents the position of peak centre and by σ_i that controls its width. This can be formulated as follows:

$$GMM = \sum_{i=1}^{k} \frac{1}{\sqrt{2\pi}\sigma_i} \exp\left(\frac{-(w - \overline{\mathbf{w}}_i)^2}{2\sigma_i^2} \right), \tag{13}$$

where w represents values assigned to the image voxels. In each iteration over k, where the value of k is between 2 (two Gaussian functions used for approximation of the normalized image histogram and differentiation between the background and object) and K, an appropriate value of $\overline{\mathbf{w}}_i$ is chosen.

First, among the $\overline{\mathbf{w}}_i$ values the ones whose contributions to approximation exceed 10%, are selected. Secondly, $\overline{\mathbf{w}}_i$ are sorted in the ascending order. If the data are enhanced by a contrast agent, the highest value of $\overline{\mathbf{w}}_i$ is chosen (the value resembling bones and tissues with a contrast). Otherwise, the penultimate value of $\overline{\mathbf{w}}_i$ (the value resembling a soft tissue, in this case also the kidney) is picked out. Next, it is checked whether the value of σ_i^2 corresponding to the chosen $\overline{\mathbf{w}}_i$ is typical for the component representing the kidney. Too high a value of σ_i^2 implies iterative continuation of the estimation process with $k = k + 1$ (probably other structures with different values are around the kidney). Finally, μ is equal to $\overline{\mathbf{w}}_i$ for the chosen k. An example of approximation of a normalized image histogram by GMM with $k = 3$ and $k = 4$ is presented in Fig. 2. In some cases fixing the μ value has to be done manually.

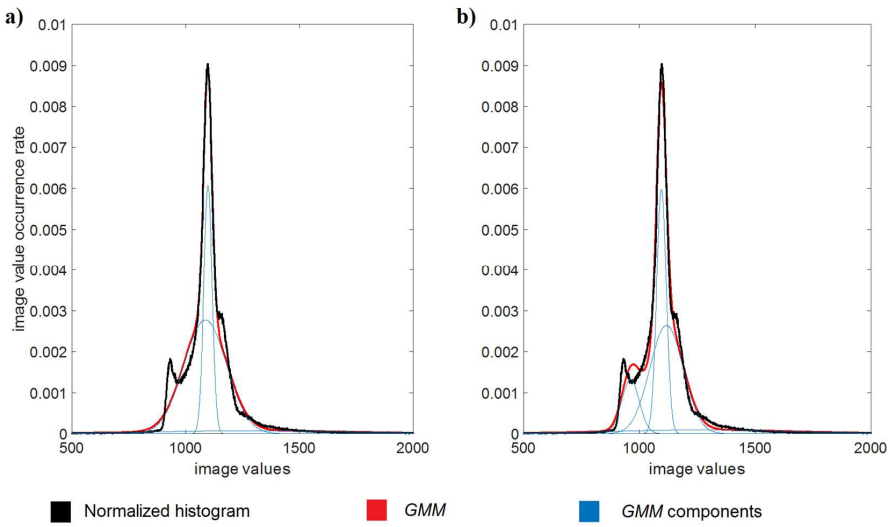

Fig. 2. An example of approximation of a normalized image histogram by GMM with $k = 3$ (a) and $k = 4$ (b). The data are without a contrast agent which implies that the penultimate value of $\overline{\mathbf{w}}_i$ is selected. In the case of (a) two Gaussian functions are meaningful, but the value of σ_i^2 corresponding to the chosen $\overline{\mathbf{w}}_i$ is too high. In the case of (b) three Gaussian functions are meaningful, and the value of σ_i^2 is appropriate.

2.6. Minimization of energy functional

The proposed functional (3) can be rewritten as:

$$E(C) = -\lambda_1 \int_{\Omega} \left(\mathbf{I}(\mathbf{x}) - \mu\right) H(\Phi) d\Omega + \lambda_2 \int_{\Omega} \mathbf{g}(\mathbf{x}) \left| \nabla H(\Phi) \right| d\Omega + \lambda_3 \int_{\Omega} \mathbf{D}^2(\mathbf{x}) \left| \nabla H(\Phi) \right| d\Omega . \tag{14}$$

By minimizing the energy functional with respect to Φ, a PDE determining the evolution of Φ (derived from the Gateaux derivative gradient flow [16]) was defined:

$$\Phi_t = \delta(\Phi)\left[\lambda_1\left(\mathbf{I}(\mathbf{x})-\mu\right)+\lambda_2\mathrm{div}\left(\mathbf{g}(\mathbf{x})\frac{\nabla\Phi}{|\nabla\Phi|}\right)+\lambda_3\mathrm{div}\left(\mathbf{D}^2(\mathbf{x})\frac{\nabla\Phi}{|\nabla\Phi|}\right)\right]. \tag{15}$$

According to [14, 21] $\delta(\Phi)$ can be replaced by $|\nabla\Phi|$:

$$\Phi_t = |\nabla\Phi|\left[\lambda_1\left(\mathbf{I}(\mathbf{x})-\mu\right)+\lambda_2\mathrm{div}\left(\mathbf{g}(\mathbf{x})\frac{\nabla\Phi}{|\nabla\Phi|}\right)+\lambda_3\mathrm{div}\left(\mathbf{D}^2(\mathbf{x})\frac{\nabla\Phi}{|\nabla\Phi|}\right)\right]. \tag{16}$$

Based on the identity $\mathrm{div}\left(\mathbf{g}\vec{\mathbf{f}}\right)=\nabla\mathbf{g}\cdot\vec{\mathbf{f}}+\mathbf{g}\,\mathrm{div}\left(\vec{\mathbf{f}}\right)$, where "$\cdot$" denotes the inner product, (16) can be written as ($\mathbf{g}=\mathbf{g}(\mathbf{x}), \mathbf{I}=\mathbf{I}(\mathbf{x}), \mathbf{D}=\mathbf{D}(\mathbf{x})$):

$$\Phi_t = |\nabla\Phi|\left[\lambda_1\left(\mathbf{I}-\mu\right)+\lambda_2\nabla\mathbf{g}\cdot\frac{\nabla\Phi}{|\nabla\Phi|}+\lambda_2\mathbf{g}\,\mathrm{div}\left(\frac{\nabla\Phi}{|\nabla\Phi|}\right)+\lambda_3\nabla\mathbf{D}^2\cdot\frac{\nabla\Phi}{|\nabla\Phi|}+\lambda_3\mathbf{D}^2\mathrm{div}\left(\frac{\nabla\Phi}{|\nabla\Phi|}\right)\right]. \tag{17}$$

Using notation $\kappa=\mathrm{div}\left(\frac{\nabla\Phi}{|\nabla\Phi|}\right)$, (17) has the following form:

$$\Phi_t = |\nabla\Phi|\left[\lambda_1\left(\mathbf{I}-\mu\right)+\lambda_2\nabla\mathbf{g}\cdot\frac{\nabla\Phi}{|\nabla\Phi|}+\lambda_2\mathbf{g}\kappa+\lambda_3\nabla\mathbf{D}^2\cdot\frac{\nabla\Phi}{|\nabla\Phi|}+\lambda_3\mathbf{D}^2\kappa\right], \tag{18}$$

where κ represents the curvature of evolving contour/surface C. The objective of this term is ensuring smoothness of the surface. The evolution is performed in the iterative way based on splitting the additive operator. The details of the numerical implementation can be found in [16].

3. Experiment and results

The CT dataset used for testing the proposed kidney segmentation framework consisted of 10 patients diagnosed with renal cancer. The data were acquired in different medical centers and therefore the examinations were performed on different devices and using different acquisition protocols. In consequence, in our dataset there are 2 CT scans with and 8 without a contrast agent injected during examination. Furthermore, the spatial resolution of data in the dataset was various (the spacing range: 0.6094–0.8848 mm, the slice thickness range 1–3 mm).

Figure 3 shows the influence of individual components on segmentation of CT data. It can be observed that lack of the ellipsoidal shape constraints on the evolving surface leads to excessive expansion to the neighboring structures. For example (Figs. 3a and 3b), after occurring a topological change, the zero-level set of Φ has propagated to ribs adjacent to the kidney (high values assigned to the voxels). Introduction of an additional boundary term resulted in reduction of divisions within the kidney only to the areas with the largest gradient (Fig. 3e). The strength of an impact of the boundary term can be adjusted via the parameter λ_2.

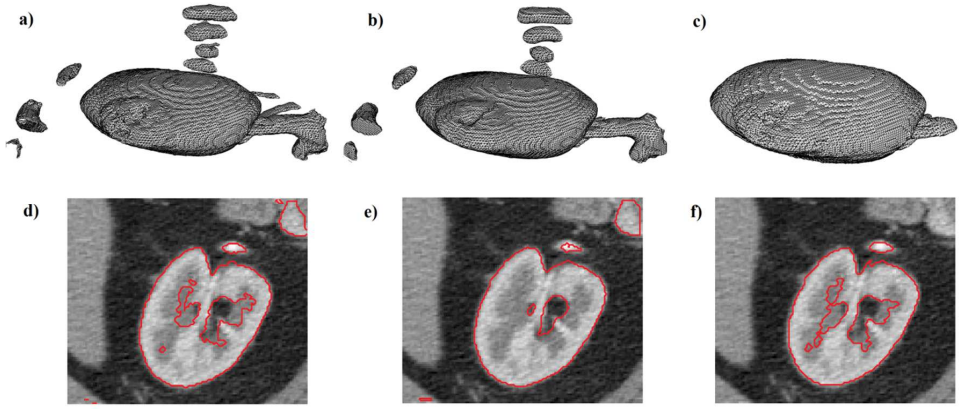

Fig. 3. The influence of energy terms. (a) to (c) visualization of three-dimensional results; (d) to (f) an example of a slice with segmentation results (red contour). (a) and (d) only the area term; (b) and (e) the area and boundary terms; (c) and (f) the area and boundary terms with the ellipsoidal shape constraint for $\mathbf{D}_{II}$ formulation.

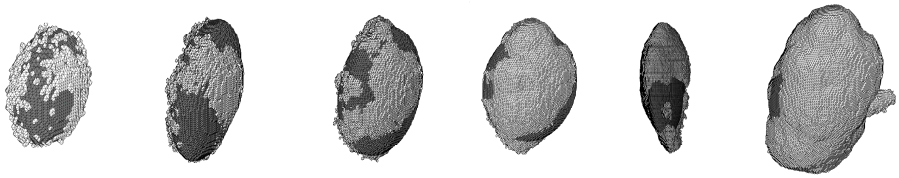

Fig. 4. The zero-level sets of Φ (light grey) and **D** (dark grey) in consecutive iterations. From left to right: iterations: 5, 10, 15, 20, 25, 35.

Additionally, the impact of shape constraint is also presented in Fig. 4. The zero-level sets of estimated shape **D** (dark grey) and function Φ (light grey) are shown on consecutive iterations.

To ensure proper validation of the segmentation results in each case the manual segmentation was performed using ITK-SNAP software [24]. In order to assess effectiveness of the segmentation, the three following measures were used: a typical volumetric measure – the Dice Coefficient (19) [25] and two Hausdorff spatial distance measures [26]: maximum $dH_{\max}$ (20) and average dH_{avg} (21).

Assuming that $\mathbf{M}_{\text{mc}}$ is a binary mask from manual segmentation and $\mathbf{P}_{\text{mc}}$ is a set of coordinates of its points, $\mathbf{M}_{\text{seg}}$ is a binary mask obtained by the algorithm and $\mathbf{P}_{\text{seg}}$ is a set of coordinates of its points, the aforementioned measures can be formulated as:

$$DICE = \frac{2\left(\mathbf{M}_{\text{mc}} \cap \mathbf{M}_{seg}\right)}{\mathbf{M}_{\text{mc}} \cup \mathbf{M}_{seg}}, \tag{19}$$

$$dH_{\max} = \max\left(h_1\left(\mathbf{P}_{\text{mc}}, \mathbf{P}_{\text{seg}}\right), h_1\left(\mathbf{P}_{\text{seg}}, \mathbf{P}_{\text{mc}}\right)\right), \tag{20}$$

$$dH_{avg} = \max\left(h_2\left(\mathbf{P}_{\text{mc}}, \mathbf{P}_{\text{seg}}\right), h_2\left(\mathbf{P}_{\text{seg}}, \mathbf{P}_{\text{mc}}\right)\right), \tag{21}$$

where: $h_1\left(\mathbf{P}_{\text{mc}}, \mathbf{P}_{\text{seg}}\right) = \max\limits_{p_{mc} \in \mathbf{P}_{mc}} \min\limits_{p_{seg} \in \mathbf{P}_{seg}} \left\| p_{mc} - p_{seg} \right\|$, $h_2\left(\mathbf{P}_{\text{mc}}, \mathbf{P}_{\text{seg}}\right) = \text{mean}\limits_{p_{mc} \in \mathbf{P}_{mc}} \min\limits_{p_{seg} \in \mathbf{P}_{seg}} \left\| p_{mc} - p_{seg} \right\|$, where $\| \ \|$ denotes the Euclidian distance.

To calculate the Hausdorff distances, the Euclidian distances between two subsets $\mathbf{P}_{mc}$ and $\mathbf{P}_{seg}$ are determined. h_1 and h_2 are formulated as the greatest and the average of all distances, respectively. In general, dH_{avg} shows the difference between manual and automatic segmentation regarding the distance. Since it is averaged over all points, it is known to be more robust and less prone to the noise characteristic of CT data. However, dH_{max} exhibits outliers. This means that even one outlier can contribute to a huge value of dH_{max}. The connection of all three presented measures enables to fully assess effectiveness of the segmentation.

The obtained results are presented in Table 1. The lower value of the *DICE* coefficient is caused by the accuracy of manual outlines related to the complex kidney structure. The manual outlines were performed slice by slice what led to further complications in the upper and lower parts of the kidney. This is a consequence of the finite spatial resolution, which hinders specification of the first and the last slices belonging to the kidney (a common phenomenon for spherical and ellipsoidal structures). Furthermore, the manual outlines included only the structure of kidney itself, without arteries, veins and the pelvicaliceal system. A segmentation algorithm sometimes appended these structures to the segmentation results, especially if the introduced contrast agent was located inside them. The obtained mean value of *DICE* coefficient is equal to 0.862 and is on a comparable level to those presented in the literature. The high value of maximum Hausdorff distance results from the fact that among the segmentation results there were vascular structures located within the kidney area (in particular, Figs. 5a, c, g, i).

Table 1. The segmentation effectiveness regarding the Dice and Hausdorff distance measures.

	DICE	dH_{max} **[mm]**	dH_{avg} **[mm]**
Mean	0.862	19.63	2.37
Standard deviation	0.039	4.99	0.62

The segmentation results in the form of 3D hull are shown in Fig. 5. In addition, Fig. 6 presents a comparison of the manual outlines and segmentation results on the 2D transversal planes.

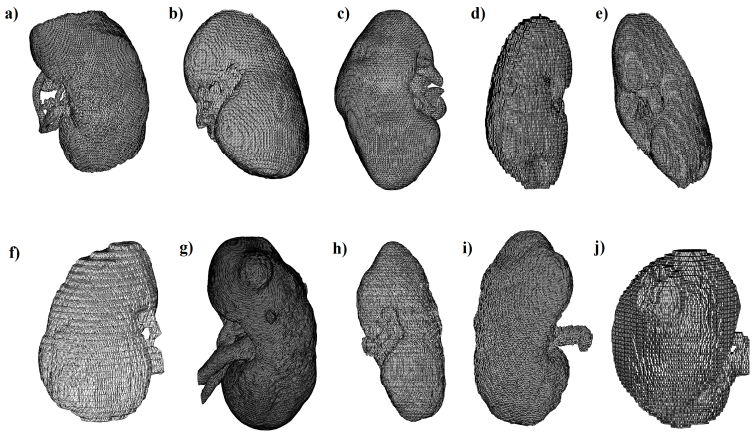

Fig. 5. The segmentation results presented as a three-dimensional model from a different angle of view and for different patients.

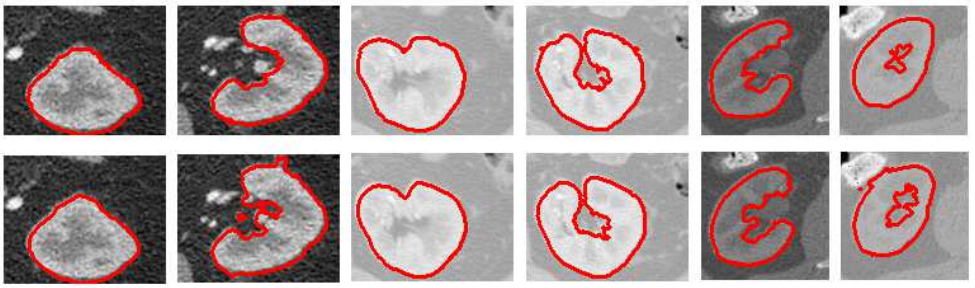

Fig. 6. A comparison of the segmentation results (second row) and manual contours (first row) presented on the transversal planes for 3 patients.

4. Conclusion

In this paper, a novel kidney segmentation algorithm using the Level Set framework with ellipsoidal shape constraints was presented. The proposed solution not only takes into account the information about the region and boundary terms, but also the constraints dedicated to the characteristic kidney shape. Thereby, an excessive growth towards undesired structures is restricted. The impact of individual energy functional terms on the segmentation process was also presented. Moreover, based on the Mixture of Gaussians, a simple and effective method for estimation of μ parameter was described (Subsection 2.5).

The proposed methodology was tested on CT scans carried out on renal cancer patients, both with and without injection of a contrast agent prior to examination. Both the quantitative (Table 1: the *DICE* coefficient equal to 0.862 ± 0.039 and the average Hausdorff distance equal to 2.37 ± 0.62mm) and qualitative evaluations presented in Fig. 5 and Fig. 6 confirm effectiveness of the proposed solution. It may constitute a significant part of the support system for planning minimally invasive treatments in oncological urology.

Further developing path of the proposed algorithm can cover examination of cross-sectional data in real-time imaging modalities used intraoperatively. The CT/MR-ultrasound fusion image guidance combined with a tracking system can assist percutaneous diagnostic and ablation procedures. Another possibility is augmentation of the laparoscopic picture by guidance provided by CT reconstructions where automatic segmentation is also required.

Acknowledgements

The work was supported by the Ministry of Science and Higher Education, Poland (Dean Grants, statutory activity).

References

[1] Klatte, T., *et al*. (2015). A literature review of renal surgical anatomy and surgical strategies for partial nephrectomy. *European urology*, 68(6), 980–992.

[2] Shao, P., *et al*. (2013). Application of a vasculature model and standardization of the renal hilar approach in laparoscopic partial nephrectomy for precise segmental artery clamping. *European Urology*, 63(6), 1072–1081.

[3] Bugajska, K., *et al*. (2015) The renal vessel segmentation for facilitation of partial nephrectomy. *IEEE SPA 2015: Signal Processing: Algorithms, Architectures, Arrangements and Applications*, 50–55.

[4] Lin, D.T., Lei, C.C., Hung, S.W. (2006). Computer-aided kidney segmentation on abdominal CT images. *IEEE Transactions on Information Technology in Biomedicine*, 10(1), 59–65.

[5] Nedevschi, S., Ciurte, A., Mile, G. (2008). Kidney CT image segmentation using multi-feature EM algorithm, based on Gabor filters. *4th International Conference on Intelligent Computer Communication and Processing*, ICCP 2008, 283–286.

[6] Yang, G., *et al*. (2014). Automatic kidney segmentation in CT images based on multi-atlas image registration. *36th Annual International Conference of the IEEE Engineering in Medicine and Biology Society* (EMBC), 5538–5541.

[7] Xu, Z., *et al.* (2015). Efficient multi-atlas abdominal segmentation on clinically acquired CT with SIMPLE context learning. *Medical image analysis*, 24(1), 18–27.

[8] Chao, J., *et al*. (2016). 3D Fast Automatic Segmentation of Kidney Based on Modified AAM and Random Forest. Accepted to *IEEE Transaction on medical Imaging.*

[9] Spiegel, M., *et al*. (2009). Segmentation of kidneys using a new active shape model generation technique based on non-rigid image registration. *Computerized Medical Imaging and Graphics*, 33(1), 29–39.

[10] Zollner, F.G., Kocinski, M., Rorvik, J. Lundervold. (2007). Towards Automatically Assessment of Kidney Volume from 3D DCE-MRI Time Courses using Active Contours. *Proc. Intl. Soc. Mag. Reson. Med.*, 15.

[11] Tsagaan, B.S.A., Kobatake, H., Miyakawa, K., Hanzawa, Y. (2001). Segmentation of kidney by using a deformable model. *Image Processing, 2001, Proceedings, 2001 International Conference on* 3, 1059–1062.

[12] Khalifa, F., *et al.* (2011). A new deformable model-based segmentation approach for accurate extraction of the kidney from abdominal CT images. *18th IEEE International Conference on Image Processing* (ICIP), 3393–3396.

[13] Huang, Y., *et al.* (2009). Multiphase level set with multi dynamic shape models on kidney segmentation of CT image. *Biomedical Circuits and Systems Conference*, BioCAS, 141–144.

[14] Chan, T.F., Vese, L.A. (2001). Active contours without edges. *IEEE transactions on Image processing*, 10(2), 266–277.

[15] Pluempitiwiriyawej, C., *et al*. (2005). STACS: New active contour scheme for cardiac MR image segmentation. *IEEE Transactions on Medical Imaging*, 24(5), 593–603.

[16] Zhang, Y., *et al*. (2008). Medical image segmentation using new hybrid level-set method. *BioMedical Visualization, 2008, MEDIVIS'08. Fifth International Conference*, 71–76.

[17] Kass, M., Witkin, A., Terzopoulos, D. (1988). Snakes: Active contour models. *International journal of computer vision*, 1(4), 321–331.

[18] Brigger, P., Hoeg, J., Unser, M. (2000). B-spline snakes: a flexible tool for parametric contour detection. *IEEE Transactions on Image Processing*, 9(9), 1484–1496.

[19] Osher, S., Fedkiw, R. (2006). *Level set methods and dynamic implicit surfaces*. Springer Science & Business Media.

[20] Hunyadi, L., Vajk, I. (2014). Constrained quadratic errors-in-variables fitting. *The Visual Computer*, 30(12), 1347–1358.

[21] Li, Q., Griffiths, J.G. (2004). Least squares ellipsoid specific fitting. *Geometric Modeling and Processing*, 335–340.

[22] McLachlan, G., Peel, D. (2000). *Finite Mixture Models. Hoboken*. NJ: John Wiley & Sons, Inc.

[23] Vese, L.A., Chan, T.F. (2002). A multiphase level set framework for image segmentation using the Mumford and Shah model. *International journal of computer vision*, 50(3), 271–293.

[24] Yushkevich, P.A., Piven, J., Hazlett, H.C., Smith, R.G., Ho, S., Gee, J.C., Gerig, G. (2006). User-guided 3D active contour segmentation of anatomical structures: Significantly improved efficiency and reliability. *Neuroimage*, 31(3), 1116–28.

[25] Dice, L. (1945). Measures of the amount of ecologic association between species. *Ecology*, 26(3), 297–302.

[26] Dubuisson, M.P., *et al*. (1994). A modified Hausdorff distance for object matching. *ICPR94*, 566–68.